Lehrstuhl für
Experimentalphysik E20

Technische
Universität
München

Fortgeschrittenenpraktikum

Versuch:

Rastertunnelmikroskopie
& Abbildung von Molekülen

Scanning Tunnelling Microscopy
& Molecular Imaging

updated July 2016

Introduction to scanning tunnelling microscopy

Scanning tunnelling microscopy (STM) is a non-destructive, surface analysis method firstly implemented in the IBM Research Laboratory, Zurich, Switzerland, in 1981 [1]. It enables atomic-scale surface characterisation and its significance was quickly recognised by the scientific community, as evidenced by the award of the 1986 Nobel Prize in Physics by one half to Gerd Binnig and Heinrich Rohrer, for their design of the scanning tunnelling microscope:

"… *It is evident that this technique is one of exceptional promise, and that we have so far seen only the beginning of its development. Many research groups in different areas of science are now in using the scanning tunneling microscope. The study of surfaces is an important part of physics, with particular applications in semiconductor physics and microelectronics. In chemistry, also, surface reactions play an important part, for example in connection with catalysis. It is also possible to fixate organic molecules on a surface and study their structures. Among other applications, this technique has been used in the study of DNA molecules.*" [2]

Notably, the other half of the prize was awarded to Ernst Ruska for his work concerning another real-space atomic scale characterisation technique, the electron microscope.

STM operation

Today, STM remains an invaluable and extremely versatile tool for surface and nanoscale science. It provided the basis for many landmark achievements, including the direct manipulation of atomic and molecular species, tunnelling spectroscopies of various kinds (elastic, inelastic or spin-polarized) and spurred the development of an entire family of scanning probe techniques (atomic force, near-field optical, magnetic force microscopy etc.).

STM utilises the quantum tunnelling effect of electrons between two (semi)conducting materials separated by vacuum or insulating barrier of limited thickness. In a nutshell, an atomically sharp metallic probe (tip) is positioned at a distance of ~ 1 nm from a (semi)conducting surface of interest by using piezo electric elements. The tip scans over the surface while a bias of the order of a few mV up to a few V is applied between the two electrodes to generate a net tunnelling current (see Figure 1). In the following we describe the principle of the quantum mechanical tunnelling effect and derive expressions for the tunnelling current. Subsequently we discuss the physical interpretation of STM micrographs, molecular imaging and additional investigations which are possible.
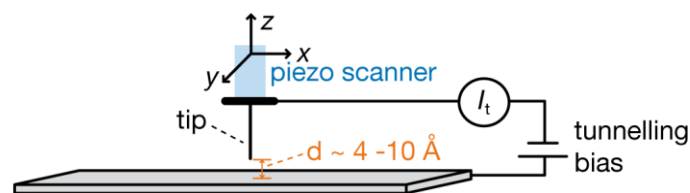

Figure 1 Schematic illustration the STM: A tip separated from a sample surface by distance d scans the surface by means of a piezo ceramic element. When a small voltage is applied between the sample and the tip, tunnelling current can be recorded.

Physical principle of tunnelling through a barrier.

Let us consider an electron of energy E and mass m, described in quantum mechanics by a wavefunction ψ, tunnelling through a one-dimensional potential barrier V_0 of width d (Figure 2). Its time-independent Schrödinger equation (TISE) can be written as

$$-\frac{\hbar}{2m}\frac{d^2\psi}{dz^2}+V\psi=E\psi$$

where $\hbar$ is Planck's constant divided by 2π, z is the spatial coordinate and V is the potential energy. Here $V=V_0$ for $0\le z\le d$ and $V=0$ for $z\le 0$ and $z\ge d$ (Figure 2).
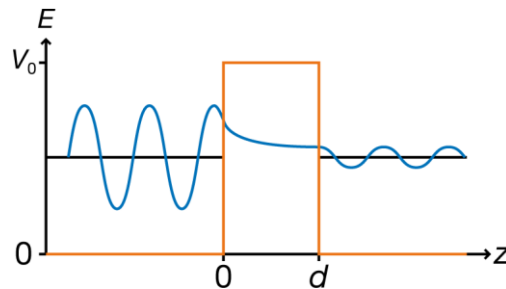

Figure 2 Schematic illustration of a wavefunction (in blue) tunnelling through a potential barrier (orange) V_0 with width d.

The general solution to the TISE is

$$\psi=\begin{cases} A_1e^{ikz}+A_2e^{-ikz} & \text{for } z\le 0 \\ B_1e^{\kappa z}+B_2e^{-\kappa z} & \text{for } 0\le z\le d \\ C_1e^{ikz}+C_2e^{-ikz} & \text{for } z\ge d \end{cases}$$

where A_1, A_2, B_1, B_2, C_1 and C_2 are constants, $k=\sqrt{\dfrac{2mE}{\hbar^2}}$ and $\kappa=\sqrt{\dfrac{2m(V_0-E)}{\hbar^2}}$. Since for $z\ge d$ we can only have waves propagating out of the potential barrier, C_2 can be set equal to zero. By imposing the continuity of the wavefunction at 0 and d, we can express the transmission coefficient as:

$$T=\left(1+\frac{\left(k^2+\kappa^2\right)^2}{4k^2\kappa^2}\sinh^2\left(\kappa d\right)\right)^{-1}$$

For a large attenuating barrier, this can be approximated as

$$T\approx\frac{16k^2\kappa^2}{\left(k^2+\kappa^2\right)^2}e^{-2\kappa d}$$

Notice that the transmission coefficient has an ***exponential*** dependence on the tunnelling barrier width.

Accordingly the tunnelling current can be expressed as:

$$I_t = C \cdot \exp(-2\kappa d) = C \cdot \exp\left(-2\frac{\sqrt{2m(V_0 - E)}}{\hbar}d\right)$$

where C is a constant.

This expression for the tunnelling current, which is based on the simple model of an individual electron passing through a potential barrier, provides a first idea on tunnelling between two solid surfaces. For electrons at the Fermi level, the workfunction Φ (see also Figure 3a) represents the minimum energy barrier to be overcome for leaving a given solid. However, by carefully approaching the two materials, controlled tunnelling currents can be generated.

Tunnelling within the sample-barrier-tip junction.

In order to have a net tunnelling current, the sample and the tip are offset by a voltage (typically from mV to less than 4 V) resulting in the band alignments illustrated in Figure 3. Therefore, with *negative sample bias we probe the filled states* of the sample surface and with *positive sample bias we probe the empty states* of the sample surface.
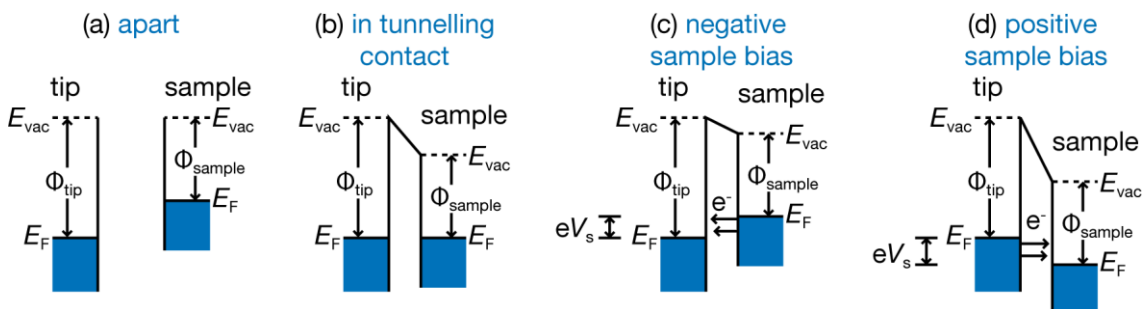

Figure 3 Schematic of the energy levels of the tip and the sample when: *(a)* they are separated and have the same vacuum level; *(b)* they are in tunnelling contact and their Fermi levels align; *(c)* they are in tunnelling contact, the sample is biased negatively, therefore its energy levels are shifted up by the bias voltage applied and this results in a net flow of tunnelling electrons from the filled states of the sample to the empty states of the tip; *(d)* they are in tunnelling contact, the sample is biased positively, therefore its energy levels are shifted down by the bias voltage applied and this results in a net flow of tunnelling electrons from the filled states of the tip to the empty states of the sample.
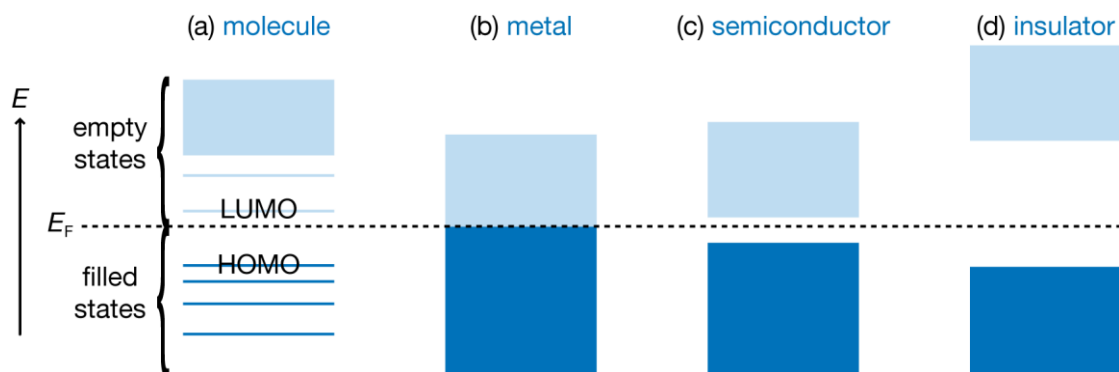

Figure 4 Schematic of the energy levels of *(a)* a molecule indicating the highest occupied molecular orbital (HOMO) and the lowest unoccupied molecular orbital (LUMO), *(b)* a metal, *(c)* a semiconductor, and *(d)* an insulator.

In a quantum mechanical description of matter, electrons have characteristic energy levels. For solid state materials the distinct energy levels that can be found in atoms or molecules merge into the band structure. Solids are classified as metallic, (semi)metallic, semi-conducting and insulating, depending on the occupation of electrons around the Fermi level (see Figure 4). For tunnelling it is imperative that there are electronic states at the energy levels accessed by the sample bias. Therefore *STM is generally not suitable for the investigation of insulating samples*.

Bardeen [3] introduced the transfer-Hamiltonian approach for approximate solutions of the exact Hamiltonian, for the time-dependent case. Within this formalism, the tunnelling current between a tip and a surface separated by an energy barrier is given by

$$I_t = \frac{2\pi e}{\hbar} \sum_{\mu,v} \left\{ f(E_\mu) \cdot [1 - f(E_v - eV_s)] - f(E_v - eV_s) \cdot [1 - f(E_\mu)] \right\} \cdot |M_{\mu v}| \cdot \delta \left(E_v - E_\mu \right)$$

where $f(E)$ is the Fermi distribution, V_s is the bias applied to the sample, $M_{\mu v}$ is the tunnelling matrix element between the states ψ_μ of the tip and the states ψ_v of the sample surface and E_μ and E_v are the eigenvalues of ψ_μ and ψ_v, respectively. The delta function ensures the conservation of energy in elastic tunnelling. For small voltages, the matrix element can be evaluated to be

$$M_{\mu v} = \frac{-\hbar^2}{2m} \int \left(\psi_\mu^* \nabla \psi_v \right) \cdot \mathrm{d}\mathbf{S}$$

where $\mathbf{S}$ is the surface area within the barrier. For low temperature the tunnelling current can be further approximated by

$$I_t = \frac{2\pi e^2}{\hbar} V_s \sum_{\mu,v} |M_{\mu v}|^2 \cdot \delta \left(E_v - E_F \right) \cdot \delta \left(E_\mu - E_F \right)$$

Tersoff and Hamann [4] considered a tip represented by a locally spherical potential well and evaluated the matrix element for an s-type tip wavefunction (Figure 5a), resulting in the tunnelling current approximation:

$$I_t \propto V_s \cdot n_t(E_F) \cdot \exp\left(2 \frac{\sqrt{2m\Phi}}{\hbar} R \right) \cdot \sum_v |\psi_v(\mathbf{r_0})|^2 \cdot \delta \left(E_v - E_F \right)$$

where Φ is the workfunction, $n_t(E_F)$ is the density of states (DOS) of the tip at the Fermi level, R is the effective tip radius and $\mathbf{r_0}$ is the centre of curvature of the tip.

Lang [5] performed calculations within the above formalism to demonstrate that *STM images a convolution of the local DOS and the topography and does not represent the true topography of the surface*. For instance, a Na atom was assumed to be scanned over a He atom at constant current, as shown in Figure 5b. This resulted in the observation of a depression, which indicates that a negative tip displacement is required in order to keep the current constant, whereas the He atom clearly has a positive height in the true topography.
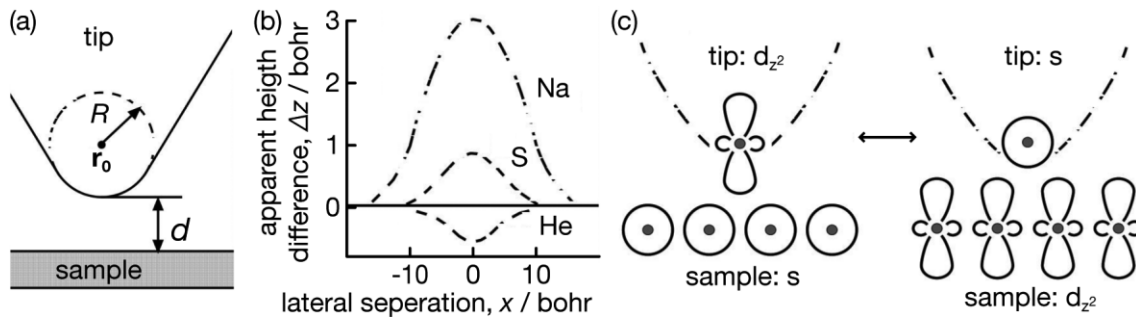
Figure 5 *(a)* Tersoff-Hamann approximation of s-type tip. *(b)* Constant-current contour line for a Na terminated metallic tip and Na/S/He adsorbate atoms on a model substrate [5]. The adsorbate atom is centred at $x = 0$ and the pristine surface plane at (an apparent) height difference 0. Note that the adsorbate atoms are physically located above the surface plane but may be imaged as depressions. (1 bohr = 0.529 Å) *(c)* Illustration of the reciprocity principle by Chen [6] which states that the tunnelling process is the same if a d_{z^2} -wave tip scans over an s-wave surface or an s-wave tip scans a d_{z^2} -wave surface.

The evaluated spatial resolution limit of STM [4, 5, 7], based on the approximations above, is inconsistent with the experimental evidence which shows that STM can give atomically resolved images. By introducing the reciprocity principle (Figure 5c), Chen [6] showed that this discrepancy arises from the assumption of an s-wave tip. The reciprocity principle states that if the tip and sample states were interchanged, the resulting STM image would remain the same. Considering that commonly used tip materials (mostly W or PtIr etc.) have d band electrons, he simulated atomically resolved corrugation by scanning an s-wave tip over a d_{z^2} -wave surface. This result accounts for the atomic resolution observed in experimental images. Chen also noted the importance of knowing the nature of the tip apex atom (tip termination), when estimating the maximum corrugation of an STM image.

Scanning modes.

In STM experiments initially the tip is carefully approached to the surface. Once the tip is close enough to the surface for a tunnelling current to be recorded, the tip scans the surface line-by-line. The tip is mounted at piezoelectric elements which are arranged in such a way that the x-y-z position of the tip is controlled with high accuracy by using precisely regulated voltages to deform the piezos. The set of data recorded is usually displayed as images, with the value of interest (apparent height, tunnelling current, tunnelling current first derivative over sample bias) displayed in two dimensions against the x and y position coordinates. Two important modes of scanning are classified: constant current mode and constant height mode.

In the *constant current mode* (Figure 6a), the height of the tip is adjusted continuously by means of a feedback loop, so that a chosen tunnelling current remains always constant. A topographic image is derived by recording the movement of the tip in the z direction. This is the most common scanning mode, as it will compensate for the surface roughness.

In the *constant height mode* (Figure 6b), the average height of the tip above the surface is constant and variations of the tunnelling current are

recorded. The principle advantage of this mode is that it does not require a quickly responding feedback loop for continuously adjusting the tip height, which slows down the imaging.
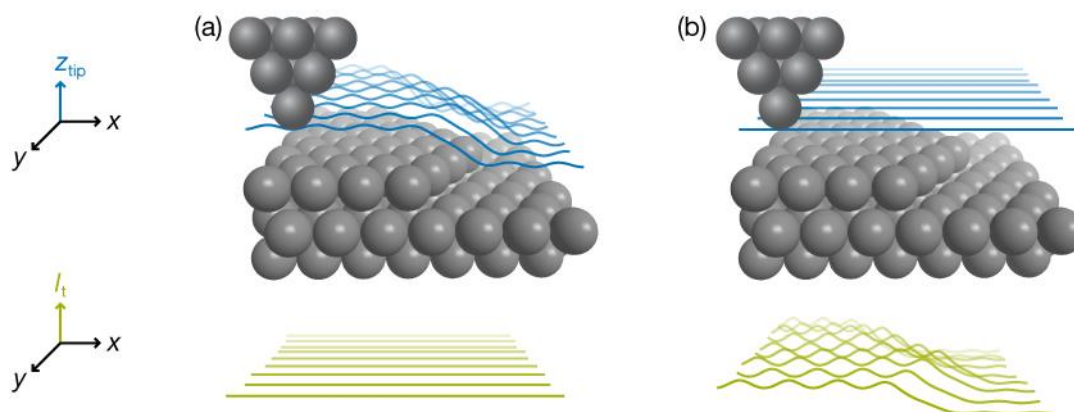

Figure 6 Schematic illustration of line scans across x showing the variation of the tip position (blue) and the tunnelling current (green) in *(a)* constant current mode and *(b)* constant height mode.

Low-index single crystal surfaces typically consist of atomically flat terraces separated by monoatomic steps. The feedback control protects the tip from physically crashing onto the surface and from losing the tunnelling contact. Note that *STM measurements can be performed in any environment, which can act as a potential barrier for tunnelling, including* **vacuum, air, various liquids and thin insulating films**.

Experimental summary

This experiment will be guided by a scientist experienced with STM. Firstly, you will probe a graphite surface: the topography and the voltage-current characteristics of the tunnelling junction in air. Subsequently you will image an organic molecule and its arrangement at the solid-liquid interface. During the experiment you are asked to keep notes of such detail that would allow a fellow student to repeat the experiment. This would correspond to a lab book entry and is an essential part of the experimental process. If it is not clear to you what should be included in this entry, discuss with your lab demonstrator.

The HOPG (0001) surface.

Graphite is an allotrope of carbon. In this experiment we use highly oriented pyrolytic graphite (HOPG), which is also suitable as a substrate for a molecular layer. It consists of flat layers of sp^2-hybridized carbon atoms in a hexagonal arrangement (nowadays called graphene sheets) with an interatomic spacing of 1.42 Å (separation a marked in Figure 7a). The graphene sheets define the (0001) plane in the crystal structure of graphite. These layers are separated by 3.35 Å. The stacking of these layers is of AB type, as shown in Figure 7a. The surface layer is rather inert in air and under typical solvents. It thus provides an excellent platform for the investigation of molecular layers with the thickness of a single molecule.

Figure 7b shows a typical STM image of this surface with atomic resolution. Around the Fermi level, the electron density is higher around the C atoms shown in white in Figure 7a, resulting in them appearing higher in the STM image (see Figure 7c). In contrast the C atoms shown in black in Figure 7a are not visible in the STM image for sample biases close to the Fermi level, *i.e.*, $|V_s| \leq 200$ mV. For a more detailed description of the HOPG (0001) STM contrast see reference [8].
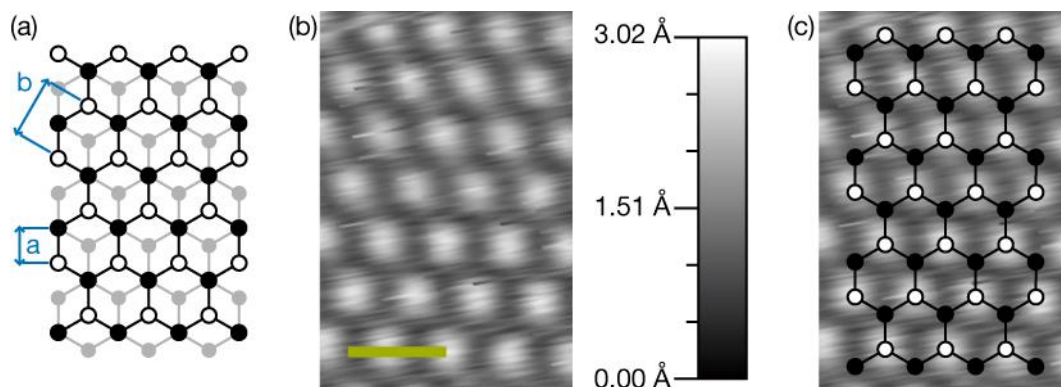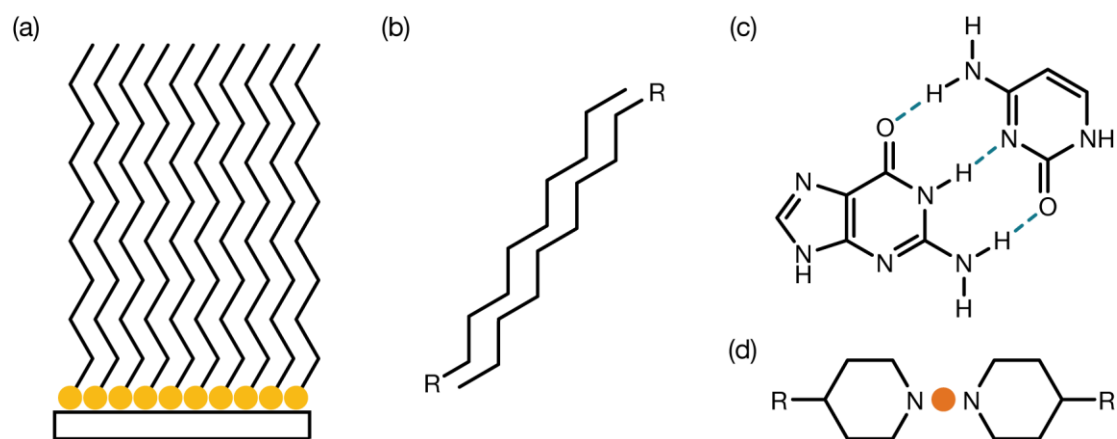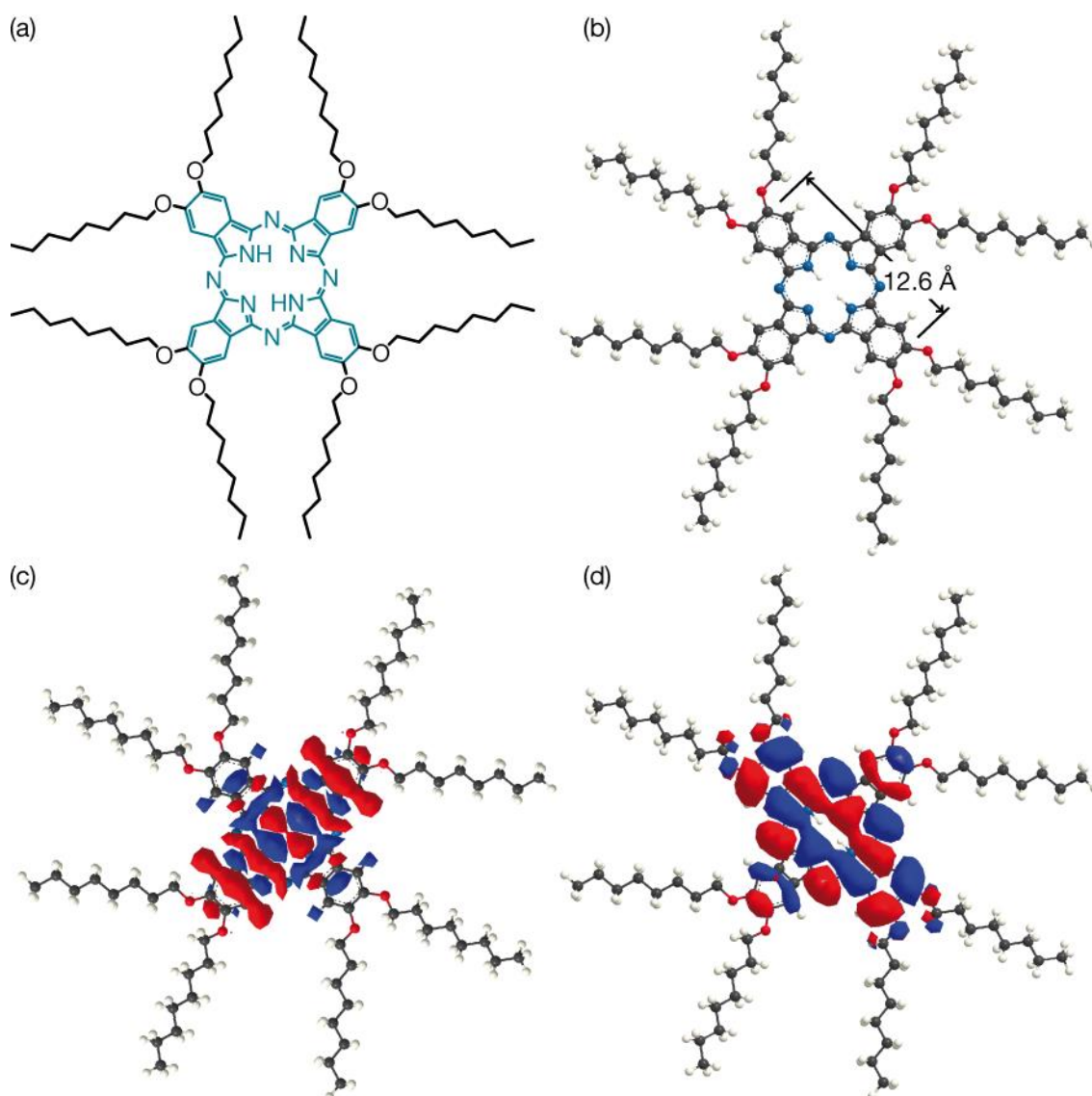

Figure 7 *(a)* Schematic illustration of the graphite structure viewed on the (0001) plane. The C atoms of the top layer are depicted in black and white whereas from the layer below they are depicted in grey. C atoms in black reside atop C atoms of the layer underneath. C-C lateral bonding distance is given by a = 1.42 Å. The (0001) surface unit cell has a side of b = 2.46 Å. *(b)* STM micrograph acquired with a chemically etched tungsten (W) tip in air at room temperature. The grey scale bar on the right shows the respective conversion of apparent height to the colour. The green scale bar marks a length of 4 Å. ($V_s = 0.23$ V, $I_t = 0.95$ nA.) *(c)* The graphite (0001) structure superposed onto the STM image shown in (b).

Molecules and self-assembled layers.

The second task of this practical training is the visualisation of phthalocyanine molecules. These are characterised by the aromatic macrocycle shown in blue in Figure 8a. The macrocycle is planar, in contrast to the aliphatic chains (black in Figure 8a) which have the freedom to rotate around each C-C or C-O bond. A ball-and-stick model is shown in Figure 8b. Figure 8c,d shows the HOMO (highest occupied molecular orbital, *cf.* Figure 4a) and the LUMO (lowest unoccupied molecular orbital, *cf.* Figure 4a) of the molecule, which are mainly localised at the macrocycle. The molecules are dissolved in 1,2,4-trichlorobenzene (TCB), which has a low dielectric constant (relative permittivity) ~ 2.2 [9]. This is needed for the solvent to play the role of the potential barrier.

Self-assembly is a key concept of natural systems and widely employed in nanoscale science, where nanostructures are created in a bottom-up approach. **Self-assembly** is defined as the order which emerges in an ensemble of building blocks near *equilibrium*, as the total system reduces its free energy. Molecules confined to the two dimensional environment (a surface) of a metal very often "self-assemble" (molecular self-assembly) [10]. A prototypical example of a self-assembled monolayer consists of alkanes functionalised with thiol head groups on the gold surface [11] (Figure 9a). However the head group chemistry is not a prerequisite for self-assembly. Non-covalent interactions (such as the examples shown in Figure 9b-d) can be utilised, resulting in *supramolecular* self-assembled structures [12].

Figure 8 *(a)* Molecular formula of the octakis-octyloxy-phthalocyanine to be investigated. The phthalocyanine macrocycle is shown in blue. *(b)* Corresponding ball-and-stick model: Carbon, nitrogen, oxygen, and hydrogen atoms are shown in dark grey, blue, red, and white, respectively. The physical dimensions of the phthalocyanine macrocycle are indicated. *(c)* The HOMO overlaid on the molecular model. *(d)* The LUMO overlaid on the molecular model.

Figure 9 *(a)* Illustration of a self-assembled monolayer: head groups (yellow circles, e.g. thiolates) chemisorb onto a substrate (rectangle below yellow circles, e.g. gold) followed

by arrangement of the tail groups (here alkanes). *(b-d)* Exemplary interactions which are utilised in supramolecular assembly: *(b)* van der Waals interaction between alkane groups, *(c)* triple hydrogen bonding scheme (blue dotted lines) (here between the DNA base pairs guanine and cytosine) and *(d)* metal centre (orange circle) coordination with the lone pairs of electrons of the nitrogen atoms in pyridine groups.

The phthalocyanine macrocycle generally bonds with its π orbitals to (semi)metallic substrates, thus resulting in a planar adsorption geometry. Although the HOPG surface does not provide strong anchoring sites for the immobilisation of the macrocycle, self-assembled layers are afforded through van der Waals interactions between alkane substituents (Figure 9b). For octakis-octyloxy-phthalocyanines on HOPG two different arrangements have been reported [13]: a quadratic (unit cell with side lengths of 2.6±0.1 nm and an angle of 90°±5° between them, Figure 10) and a pseudo-hexagonal (unit cell with side lengths of 2.6±0.1 nm, 2.7±0.1 nm and an angle of 65°±5° between them).
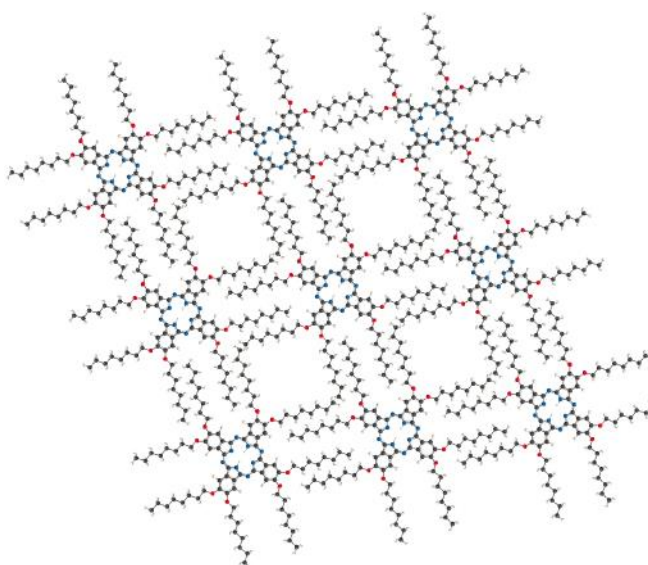

Figure 10 Molecular model of the quadratic arrangement of octakis-octyloxy-phthalocyanines on HOPG based on STM images. (Adapted from ref. [14].)

Probing the HOPG surface

1. A fresh tip will be prepared by mechanical cutting and simultaneously applying a shearing tension. It is positioned on the STM scanner.
2. A fresh layer of HOPG surface is prepared by exfoliating the top layers using scotch tape. The sample is mounted on the STM stage.
3. Approach the tip towards the HOPG surface in air.
4. Investigate the topography of HOPG in constant current mode. You should achieve atomic resolution in the topography images of HOPG.
5. Record current *versus* distance spectra at different locations with initial tunnelling current of 10 pA at three different biases: 10 mV, 200 mV, and -200 mV.
6. Record current *versus* voltage spectra with initial tunnelling conditions of ~ 10 pA and 200 mV over a range of 200 mV to -200 mV.

Direct visualisation of phthalocyanines at the HOPG/TCB interface

1. Topographic STM images of (20 nm)^2 showing phthalocyanine molecules are to be recorded after retracting the tip and dropping ~ 4 µL of a

phthalocyanine solution in TCB. Use the following approach parameters: set point of 10 pA and sample bias of 200 mV.

After the laboratory

To complete this practical course you will need to submit a written report and take an oral examination.

Report

The report should consist of a brief description of the experiment, your measurements and observations, and a brief summary of your findings.
The following should be addressed within this report.

- Characterise the topography of the HOPG surface. Identify and measure the unit cell. One can use the fast Fourier transformation (FFT) function to convert from real space to reciprocal space lattice. (This allows a measurement of the periodic ensemble.) How do these values compare to the expected ones? Do you observe any experimental lateral drift? What is its origin? Calibrate the lateral dimensions of the STM image.
- Use the tunnelling current versus height measurements to estimate the parameter κ of the HOPG/air/tip system. Do you observe a dependence of the tunnelling current versus height upon the initial tunnelling bias? Why? Estimate the tunnelling barrier height. In the STM junction the barrier height can be approximated to the average workfunction of the tip and the sample surface. How does it compare with the value obtained from your measurements? (The work function of the HOPG surface is measured to be 4.4 eV [15] whereas of the Pt/Ir tip is close or greater to 5.2 eV [16].)
- Display the tunnelling current versus voltage curves corresponding to HOPG. What information does this give for the electronic structure of graphite?
- Identify the molecular features of the phthalocyanine molecules in the topography images. Which parts appear brighter and why?
- Describe the supramolecular assembly of the molecules. Give a crystallographic description of the arrangement. What are the interactions of the molecules within the observed network?

Colloquium

You will be asked on the operation principle of the STM, the practical implementation and the physical information you can derive by STM.

REFERENCES

1. G. Binnig and H. Rohrer, 'Scanning tunneling microscopy—from birth to adolescence' *Rev. Mod. Phys.*, 1987. **59**(3): 615-625.
http://link.aps.org/doi/10.1103/RevModPhys.59.615

2. 'Press Release: The 1986 Nobel Prize in Physics'. Nobelprize.org
http://www.nobelprize.org/nobel_prizes/physics/laureates/1986/press.html

3. J. Bardeen, 'Tunnelling from a many-particle point of view' *Phys. Rev. Lett.*, 1961. **6**(2): 57-59. http://link.aps.org/doi/10.1103/PhysRevLett.6.57

4. J. Tersoff and D.R. Hamann, 'Theory of the scanning tunneling microscope' *Phys. Rev. B*, 1985. **31**(2): 805-813. http://link.aps.org/doi/10.1103/PhysRevB.31.805

5. N.D. Lang, 'Vacuum tunneling current from an adsorbed atom' *Phys. Rev. Lett.*, 1985. **55**(2): 230-233. http://link.aps.org/doi/10.1103/PhysRevLett.55.230

6. C.J. Chen, 'Origin of atomic resolution on metal surfaces in scanning tunneling microscopy' *Phys. Rev. Lett.*, 1990. **65**(4): 448-451. http://link.aps.org/doi/10.1103/PhysRevLett.65.448

7. N.D. Lang, 'Theory of single-atom imaging in the scanning tunneling microscope' *Phys. Rev. Lett.*, 1986. **56**(11): 1164-1167. http://link.aps.org/doi/10.1103/PhysRevLett.56.1164

8. E. Cisternas, F. Stavale, M. Flores, C.A. Achete, and P. Vargas, 'First-principles calculation and scanning tunneling microscopy study of highly oriented pyrolytic graphite (0001)' *Phys. Rev. B*, 2009. **79**(20): 205431. http://dx.doi.org/10.1103/PhysRevB.79.205431

9. 'Handbook of Chemistry and Physics' 87 ed, ed. D.R. Lide. 2007: CRC Press

10. J.V. Barth, 'Molecular architectonic on metal surfaces' *Annu. Rev. Phys. Chem.*, 2007. **58**(1): 375-407. http://dx.doi.org/10.1146/annurev.physchem.56.092503.141259

11. J.C. Love, L.A. Estroff, J.K. Kriebel, R.G. Nuzzo, and G.M. Whitesides, 'Self-assembled monolayers of thiolates on metals as a form of nanotechnology' *Chem. Rev.*, 2005. **105**(4): 1103-1170. http://dx.doi.org/10.1021/cr0300789

12. J.-M. Lehn, 'Supramolecular chemistry—Scope and perspectives molecules, supermolecules, and molecular devices (Nobel lecture)' *Angew. Chem., Int. Ed. Engl.*, 1988. **27**(1): 89-112. http://dx.doi.org/10.1002/anie.198800891

13. X. Qiu, C. Wang, S. Yin, Q. Zeng, B. Xu, and C. Bai, 'Self-assembly and immobilization of metallophthalocyanines by alkyl substituents observed with scanning tunneling microscopy' *J. Phys. Chem. B*, 2000. **104**(15): 3570-3574. http://dx.doi.org/10.1021/jp993501j

14. X. Qiu, C. Wang, Q. Zeng, B. Xu, S. Yin, H. Wang, S. Xu, and C. Bai, 'Alkane-assisted adsorption and assembly of phthalocyanines and porphyrins' *J. Am. Chem. Soc.*, 2000. **122**(23): 5550-5556. http://dx.doi.org/10.1021/ja994271p

15. H. Ago, T. Kugler, F. Cacialli, W.R. Salaneck, M.S.P. Shaffer, A.H. Windle, and R.H. Friend, 'Work functions and surface functional groups of multiwall carbon nanotubes' *J. Phys. Chem. B*, 1999. **103**(38): 8116-8121. http://dx.doi.org/10.1021/jp991659y

16. M. Pomerantz, A. Aviram, R.A. McCorkle, L. Li, and A.G. Schrott, 'Rectification of STM current to graphite covered with phthalocyanine molecules' *Science*, 1992. **255**(5048): 1115-1118. http://science.sciencemag.org/content/255/5048/1115.abstract